Applied Geochemistry 65 (2016) 73–86

Contents lists available at ScienceDirect

Applied Geochemistry

journal homepage: www.elsevier.com/locate/apgeochem

Reductive weathering of black shale and release of barium during hydraulic fracturing

Devon Renock*, Joshua D. Landis, Mukul Sharma

Department of Earth Sciences, Dartmouth College, Hanover, NH 03755, USA

ARTICLE INFO

Article history:
Received 6 May 2015
Received in revised form
28 October 2015
Accepted 2 November 2015
Available online 11 November 2015

Keywords:
Barium
Barite
Hydraulic fracturing
Marcellus Shale

ABSTRACT

Hydraulic fracturing is an important technological advance in the extraction of natural gas and petroleum from black shales, but water injected into shale formations in the fracturing process returns with extraordinarily high total-dissolved-solids (TDS) and high concentrations of barium, Ba. It is generally assumed that high TDS comes from the mixing of surface water (injected fluid) with Na–Ca–Cl formation brines containing elevated Ba, but the mechanisms by which such mixing might occur are disputed. Here we show that Ba in water co-produced with gas could originate from water-rock reactions, with Ba levels observed in produced waters reached on a time scale relevant to hydraulic fracturing operations. We examined samples from three drill cores from the Marcellus Shale in Pennsylvania and New York to determine the possible water-rock reactions that release barium during hydraulic fracturing. Two samples, one containing microcrystalline barite ($BaSO_4$) and one without barite, contain elevated concentrations of Ba relative to the crustal average for shale rocks. A third sample is slightly depleted in Ba relative to the crustal average. Micro-XRF measurements and SEM/EDS analysis combined with chemical sequential extraction methods reveal that a majority of the Ba in all samples (55–77 wt.%) is present in clays and can only be leached from the rock by dissolution in hydrofluoric acid. Thus, a majority of barium in our samples is relatively inaccessible to leaching under hydraulic fracturing conditions. However, the balance of Ba in the rocks is contained in phases that are potentially leachable during hydraulic fracturing (e.g., soluble salts, exchangeable sites on clays, carbonates, barite, organics).

We next studied how shale reacts with water at elevated temperatures (80 °C), low Eh (−100 to −200 mV), and a range of ionic strengths (IS = 0.85–6.4) that emulate conditions prevalent at depth during hydraulic fracturing. Our experimental results indicate that the amount of Ba released from the bulk rock has a positive correlation with the ionic strength of the reacting fluid. Between 5 and 25% of the total Ba in the rock can be leached from shale under ionic strength conditions and leachate compositions typical of produced waters over a contact time of just 7 days. We suggest that reductive weathering of black shale occurs during hydraulic fracturing due to: 1) Ba^{2+} in clays exchanging with Na^{+} and Ca^{2+} ions that are present in high concentrations in produced water, and 2) increased solubility and dissolution kinetics of barite under high ionic strength conditions. At the low Eh conditions prevalent during hydraulic fracturing the sulfate deficient water allows Ba to be dissolved into the produced water. Based on Ba yields determined from laboratory leaching experiments of Marcellus Shale and a reasonable estimate of the water/rock mass ratio during hydraulic fracturing, we suggest that all of the Ba in produced water can be reconciled with leaching directly from the fractured rock.

© 2015 Elsevier Ltd. All rights reserved.

1. Introduction

Water co-produced with gas (i.e., flowback and produced water) following the hydraulic fracturing of the Marcellus Shale (MS) has a peculiar chemical composition. While the major dissolved ions are sodium, calcium and chloride, the produced water can reach salinities that are 10 × greater than seawater with total dissolved solid (TDS) content often exceeding 150,000 mg/L (or ppm) (Blauch et al., 2009; Chapman et al., 2012; Haluszczak et al., 2013). Produced water contains appreciable amounts of other dissolved ions, as well, including magnesium, strontium, barium, uranium, radium, arsenic, vanadium, and molybdenum. Barium (Ba) and especially

* Corresponding author.
E-mail address: Devon.J.Renock@Dartmouth.edu (D. Renock).

http://dx.doi.org/10.1016/j.apgeochem.2015.11.001
0883-2927/© 2015 Elsevier Ltd. All rights reserved.

radium (Ra) are of particular concern due to their toxicity in drinking water (Baldi et al., 1996; EPA, 2014; Warner et al., 2013; Zhang et al., 2015a); Barium and Ra are alkaline earths and their geochemical behaviors are similar. Barium concentrations and Ra activities in produced water: 1) have been shown to increase over days following the start of pumping exceeding 1400 mg/L (Ba) after only 7 days of pumping and reaching activities of 5000–16,000 pCi/L (Ra), and 2) are often strongly correlated with total dissolved solids (TDS) (Chapman et al., 2012; Rowan et al., 2011; Warner et al., 2012). High concentrations of Ba^{2+} and Ra^{2+} in produced water is also problematic due to the possibility of precipitation of highly-insoluble scale-forming barite, $BaSO_4$, upon mixing with sulfate-bearing surface water (Hamlat et al., 2003; Zhang et al., 2015a). The barite thus formed sequesters available Ra^{2+} ions and forms radioactive radiobarite, $(Ba,Ra)SO_4$ (Zhu, 2004). The source and fate of Ba thus becomes important to understand if we wish to consider ways of reducing its production during Marcellus gas extraction. The key questions that must be resolved are: 1) what are the source phases of Ba in the MS, and 2) what mechanisms govern its release from each phase into produced water?

The generation of highly saline produced waters is widely assumed to occur through the mixing of injected fluid with formation water or 'basin brine', based on binary mixing models (i.e., Br–Cl, Na–Ca, TDS, and oxygen isotopes) of injected fluid with a homogeneous basin brine end-member (Capo et al., 2014; Rowan et al., 2015; Warner et al., 2012). Appalachian basinal brines are thought to permeate the MS and adjacent rock units and are generally thought to be derived from a concentrated end member comprised of residual Paleozoic seawater expelled from the Salina group (Silurian) based on observed chloride and bromide relationships (Chapman et al., 2012; Dresel and Rose, 2010; Osborn and McIntosh, 2010, 2012; Stueber and Walter, 1991; Warner et al., 2012). In this model, fluid migration throughout the basin dissolves salts and mixes with or incorporates capillary-bound relict seawater via a mechanism such as that proposed by Balashov et al. (2015). Heterogeneities in brine geochemistry in the Appalachian Basin also suggest varying stages of alteration due to water-rock interactions (e.g., dolomitization of carbonates, sulfate reduction, brine-aquifer rock interactions, and dilution (Dresel and Rose, 2010; Osborn and McIntosh, 2010, 2011; Warner et al., 2012)). Brines in permeable host formations ranging in age from Ordovician to Devonian have been reported to contain up to a few thousand ppm Ba (Dresel and Rose, 2010). A possible explanation for such high Ba concentrations is sulfate deficient brines reacting with Ba-containing minerals in the rock (e.g., silicates and carbonates) (Dresel and Rose, 2010). However, the mechanism and rates of these reactions are considered highly speculative.

Multiple episodes of brine migration in the Marcellus Formation have been documented with events dating back to basin subsidence in response to the Alleghenian orogeny (Evans, 1995). Due to the low permeability of the black shale matrix, brine migration into the MS most likely occurred through horizontal and vertical fractures within the unit. The physical and chemical nature of brines within the MS is not well known. These brines are variously described as adsorbed water films on clays, capillary water, or free-flowing brine. Desiccation of brines can also leave dried salt residues along prior fluid conduits. A schematic illustrating the potential sources of brine and mechanisms by which brines or dried salts are incorporated into injected fluids and returned to the surface as produced water is shown in Fig. 1. Incorporation of ions into Ba-free injected fluid is thought to occur either when fractures induced by hydraulic fracturing cross pre-existing fractures that have been conduits for brine migration, or when injected fluid dissolves autochthonous salts within the MS itself (Blauch et al., 2009; Capo et al., 2014; Rowan et al., 2015; Warner et al., 2012).

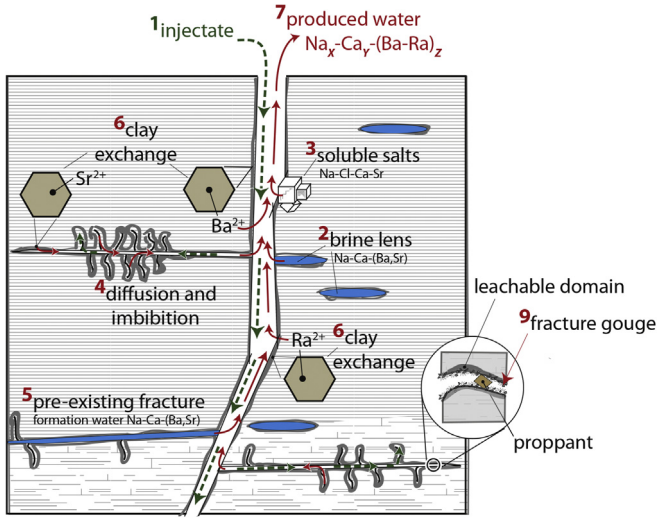

Fig. 1. Possible mechanisms contributing to the generation of produced water alkaline-earth (i.e., Ca, Sr, Ba, Ra) cation composition. These include: (1) injected fluid containing Na and Ca if recycled from previous wells; (2) hydrofracture crossing pre-existing formation water conduit (Warner et al., 2012); (3) brine inclusion in discrete lens, e.g., (Capo et al., 2014); (4) diffusion of capillary-water from pores, e.g., (Balashov et al., 2015) and imbibition of injected fluids (Engelder, 2012); (5) dissolution of soluble salts, e.g., halite (Blauch et al., 2009); (6) Ba and Ra released from leachable domain by cation exchange between host rock and saline leachate (e.g., Renock et al. herein); (7) inset shows micro-fracture with proppant (sand) and fracture 'gouge', pulverized shale which may greatly increase reactive surface area and leachable domain in the fracture zone; (8) produced water with composition determined by multiple sources and processes, and concentrations increased by factors, X Y and Z.

However, well logs and other observations indicate that MS contains very minor amounts of free brine (Engelder, 2012; Engelder et al., 2014). In response, Balashov et al. (2015) propose a model in which salt concentration, including Ba, in produced water is explained by diffusion from capillary-bound brine in the shale matrix into the injected fluid.

None of the proposed scenarios for Ba enrichment in produced water include the role of contemporaneous water-rock interactions, though others have suggested that water-rock interactions may be relevant for other elements. For example, Chapman et al. (2012) suggest that modification of formation brines by radiogenic clays in the MS is required to explain Sr isotopic composition in flowback water. Similarly, while Rowan et al. (2015) conclude that flowback salinity is derived from formation brine, they also observed that the Ra isotopic signature of the MS, specifically, is imprinted on flowback water from this unit. We consider the occurrence of Ra isotopes in flowback to be unequivocal evidence for a significant role of water-rock interactions in generating the composition of Marcellus produced water. Due to the short half-lives of ^{226}Ra (1600 years) and ^{228}Ra (5.8 years), radium isotope activity in the Marcellus formation must be supported by radioactive decay from their precursors $^{238}U > {}^{230}Th$ and ^{232}Th, respectively. The activity of U and Th in seawater is very low (Chen et al., 1986), and given its half-life restrictions, Ra occurrence in MS flowback cannot be explained by its inheritance from paleo seawater. Furthermore, preliminary Ra isotopic measurements of shale leachates are incompatible with a dispersed, soluble Ra source to produced water (Landis et al., 2015). Instead, Ra isotope activity must be supported by U and Th decay within the formation rock. Leaching of Ra from shale, even if occurring over long time scales of contact between rock and a pre-existing brine, versus the short timeframe of hydraulic fracturing, is more than a matter of semantics. It argues for active leaching of the host rock, and in this case the rates of leaching reactions become of paramount relevance to our understanding of the generation of produced water composition.

Leaching rates will depend on the solid phase speciation of Ba in the host rock, and thus an improved understanding of Ba provenance in black shale is central to our understanding of produced water chemistry. Previous studies report that total barium concentration is variable within the MS; being either depleted or enriched relative to the average shale Ba concentration of 580 ppm (Wedepohl, 1971) depending on factors such as productivity of the depositional basin, deposition rate and diagenetic processes (Lash and Blood, 2014; Niu et al., 2015 in review; Werne et al., 2002). For reference, Lash and Blood (2014) report Ba concentrations in the Oatka Creek Member of MS from Green County, PA, between 580 and 1000 ppm, but also discrete intervals that are ≥10,000 ppm. High concentrations in these intervals are often associated with the presence of macro-to micro-scale barite crystals in the rock. However, it is not well understood what solid phases Ba resides in other than barite, or what controls variations in Ba concentration within MS. Stewart et al. (2015) show that more Ba is associated with cation exchangeable sites in MS (dry-drilled cuttings from Tioga County, NY) than with soluble salts or carbonates, but the total Ba concentration in the cuttings was not reported. A study by Phan et al. (2015) on MS (dry-drilled cuttings from Tioga County, NY and Green County, PA) report bulk inventories of Ba and show that 9–74% of the total Ba in MS comprises a cation-exchangeable fraction. An important conclusion of the latter two studies is that the amount of exchangeable barium varies widely and that Ba availability and susceptibility to leaching is highly variable among MS from different geographic locations and depths within same well (Phan et al., 2015). Therefore, a comprehensive understanding of Ba enrichment in produced water requires an understanding of the solid-phase speciation of Ba in the host rock and the rates and mechanisms of Ba release from host phases under conditions relevant to hydraulic fracturing.

In this study, we consider mechanisms by which Ba may be leached directly from host phases in the rock into produced water under anoxic and high salinity conditions. We set out to determine whether Ba release rates are sufficient to explain the levels of Ba observed within days and weeks following the hydraulic fracturing of a MS well. We begin with an investigation of Ba content and mineralogy in pristine drill core samples of organic-rich MS using solid-phase analytical techniques including microscopy, X-ray diffraction (XRD), and micro X-ray fluorescence spectroscopy (μXRF). We then use chemical extractions to probe the susceptibility of Ba to leaching from the shale. Based on observations of mineralogy and susceptibility of relevant Ba-host phases, we discuss reaction mechanism(s), thermodynamics, and kinetics of water-rock reactions that release Ba from MS. We discuss the results in terms of the water/rock mass ratio in order to scale our results from the laboratory to the spatial scale expected during hydraulic fracturing.

2. Methods

2.1. Sample selection

To examine water-rock reactions we required samples of MS that have not undergone oxidative leaching due to weathering at the surface. We obtained three drill core samples from wells in New York (×2) and Pennsylvania (×1). New York and Pennsylvania core samples were obtained from the core repository at the NY State Museum, Albany, NY and the PA Department of Conservation and Natural Resources core repository, Pittsburgh, PA, respectively. All cores were obtained from the vertical leg of the well. The authors were not present during drilling. These samples have high organic content and Ba concentrations that span the range of values that are typically found in the organic-rich MS units underlying central NY and southwestern PA (see Table 2). Though these samples were not obtained from wells currently under development for gas production, they are located in rock units known to accumulate natural gas based on thermal maturity estimates assessed from vitrinite reflectance values (Weary et al., 2001). At the time of this study, New York State prohibits high-volume hydraulic fracturing. The location and approximate depth of each sample used in this study is shown in Table 1 along with an abbreviation that will be used to refer to the sample. For example, the sample from Chenango County, NY, is identified throughout the remainder of the text as "CC". Fig. 2 shows the approximate locations of each of the samples in our study (CC, YC, and IC) section. Stratigraphically, CC belongs to lower part of the Oatka Creek Formation overlying the Onondaga Formation (see detailed description in (Niu et al., 2015 in review)) along with YC. IC belongs to the Marcellus Formation overlying the Hunterville Chert (Onondaga equivalent) (Wilhelm and Cobb, 1981).

2.2. Preparation and characterization of Marcellus Shale samples

2.2.1. Microscopic and spectroscopic characterization

Thin sections (27 mm × 46 mm × 30 μm) were specially prepared under nonaqueous conditions to minimize oxidation. Scanning Electron Microscopy (SEM) and Energy Dispersive Spectroscopy (EDS) was performed using a TM-3000 SEM (Hitachi) retrofitted with an EDS Silicon Drift Detector (Bruker) located in the Dartmouth College Earth Sciences Department. The TM-3000 operates under low vacuum, so it was not necessary to coat the samples with either gold or carbon. Backscattered electron images of minerals and their various morphologies were obtained using a 15 kV electron beam. Elemental maps were generated using a μ-XRF spectrometer (Bruker M4 Tornado) with a X-ray tube source operated at 20 kV.

2.2.2. Whole rock powder characterization

For all samples, approximately 0.5 cm of the outer rim of the core was removed with a file to minimize any oxidation that may have occurred during drilling. MS core samples weighing about 0.5 kg were first broken to obtain fresh interior pieces, which were then selected and crushed to ~5 μm size with a tungsten carbide ring-mill, which was mounted in a shatter-box. To avoid cross contamination between samples during crushing, high purity SiO_2 was crushed and discarded between the samples. The mill was then "primed" by crushing a portion of the sample, which was then discarded. Following this step, the rest of the sample was crushed yielding about 100 g of powdered sample. The single-point BET surface area of the powdered samples was measured using a Micromeritics Flowsorb surface area analyzer. Shale powder particle-size distribution was estimated by the laser-scattering method using a Coulter LS230. Samples were prepared for XRD by grinding the shale in methanol for 5 min using a McCrone Mill. Samples were mixed with a 20% pure corundum internal standard (American Elements). X-ray diffraction spectra were obtained using a Bruker D8-Focus diffractometer and copper Kα source. The powdered samples were run from 2 to 70° two theta at 40 kV and 40 Ma (0.01° step increments at 2 s/step). The X-ray data were analyzed using Bruker EVA pattern processing software and quantitative analyses was performed using the software program, Rock Jock, and methods described in Srodon et al. (2001).

Finally, the samples and standards were dissolved with mixed acids HF-$HClO_4$ at elevated temperature and pressure with additions of HNO_3–H_2O_2 to fully remove refractory organic phases. Major and trace elements were measured by Inductively Coupled Plasma Optical Emission Spectroscopy (ICPOES, Thermo Iris Intrepid II) and ICP Mass Spectrometry (ICPMS, Agilent 7500c) on dilute solutions in 5% HNO_3.

Table 1
Locations and depths of Marcellus Shale samples used in this study.

Core description	Core abbreviation	Location	Depth (m)
Chenango County, NY	CC	42°40′ 20.58″ N 75° 41′ 58.50″ W	571.2–571.5
Morton salt core#13174; Yates County, NY	YC	42°34′17.69″ N 76°56′3.08″ W	349–356
Indiana County, PA	IC	40°41′6.27″ N 79°6′34.88″ W	~2418

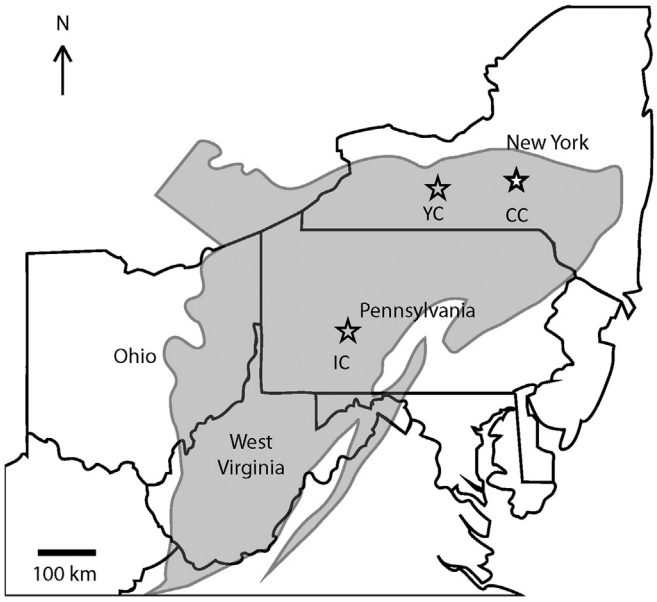

Fig. 2. Map showing location of wells where samples were recovered in New York and Pennsylvania. Shaded area shows extent of Marcellus Shale in the region.

2.2.3. Sequential extractions and barium speciation

Mineralogical speciation of barium in the powdered shale was assessed using a sequential extraction procedure. Each chemical extraction step targets a major sedimentary fraction of the shale (Eagle et al., 2003), leaving only a final residue of insoluble barite particles and a few refractory mineral phases (e.g., rutile, zircon, and metal oxides as determined by SEM/EDS of residue). Extractions were performed at an extractant:water ratio of 6:1. Extraction steps included: 1) pure deionized water (D.I., 18 MΩ) to target soluble salts (designated F1); 2) 1 M $CaCl_2$ to target the cation-exchangeable fraction (e.g.,, isovalent Ca^{2+} exchange with Ba^{2+} from clay surfaces) (F2); 3) 4 M acetic acid to target the carbonate fraction (F3); 4) 30% hydrogen peroxide, adjusted to pH ~1.5 with HNO_3, to target the oxidizable fraction, which includes both organics and sulfides (F4); 5) 0.2 M hydroxylamine in 25% acetic acid to target reducible species, e.g., oxides (F5); 6) five increasing concentrations of hydrofluoric acid in a dilute HNO_3 mixture to target silicate minerals (F6a); and saturated $AlCl_3$ in 0.1 N HNO_3 to re-dissolve fluorides formed in the preceding steps (F6b). Following each extraction, samples were rinsed in deionized water and centrifuged 3× to remove traces of preceding extractant and its chemical signature before proceeding with the next extractant. Following extractions, all samples and rinses were immediately acidified to 3% HNO_3 to prevent $BaSO_4$ precipitation during storage and prior to analysis.

Barite abundance in the refractory residue was determined chemometrically by measuring its Ba content, assuming $BaSO_4$ stoichiometry. Complete barite dissolution was achieved using Curie's carbonate-replacement (F7) method as described by Cohen and Onions (1991). Briefly, barite was boiled in a 0.5 M Na_2CO_3 solution forming a barium carbonate that was subsequently dissolved in concentrated HNO_3. Alternating carbonate-HNO_3 acid treatments were repeated until there was no Ba in leachate and SEM/EDS micrographs of the residue showed no remaining barite. Complete dissolution of a pure, synthetic $BaSO_4$ standard, processed in parallel to samples, confirmed total dissolution of insoluble sulfates (Ba yield 100 ± 2%). A mixed acid HNO_3–HCl–HF digestion of the insoluble residue targeted refractory phases (F8).

Barium and major elemental concentrations in all sequential extraction steps and rinses were determined in filtered (0.2 um), dilute HNO_3 solution using ICP-OES. Total step yields are presented as sums of the extraction and subsequent rinse steps, with cumulative uncertainties propagated by standard methods. Further details of each extraction step are given in Supplementary Information.

2.2.4. Anoxic water-rock interaction experiments

Extraction of a significant percentage of gas from extremely low permeability MS requires comminuting (i.e., fragmentation, pulverization and crushing) the shale stratum by cracks of sub-centimeter spacing (Bazant et al., 2014), which would create a range of particle sizes with a power-law distribution. Interaction of water used in hydraulic fracturing with the *finest* particles that have the largest surface-area-to-mass ratio may then impact its chemistry. Hence, to emulate water-rock interaction conditions during hydraulic fracturing, finely crushed samples of shale were reacted with water whose ionic strength was varied by adding Na and Ca salts. The experiments were performed under anoxic conditions (Eh = −100 mV to < −300 mV) and at T = 80 °C to simulate conditions during water-rock reactions occurring during hydraulic fracturing. The temperature condition is based on the maximum depths (10,000 feet or 3 km) reported for hydraulic fracturing in the Marcellus basin and assuming a geothermal gradient of 25 °C/km. Rowan et al. (2015) similarly report reservoir temperatures of ~75 °C at 8000 feet depth in Marcellus wells. Redox conditions are inferred from the predominance of anaerobic bacteria present in flowback water from Marcellus wells in Pennsylvania (Akob et al., 2015; Cluff et al., 2014). Experiments were performed using solutions with increasing ionic strengths as NaCl and $CaCl_2$, consistent with salinities reported for produced waters containing elevated Ba from Marcellus wells (Gregory et al., 2011; Rowan et al., 2015). A constant water/rock (*W/R*) powder mass ratio of 50:1 was used for all experiments.

All experiments were carried out in an anoxic chamber (Coy) which provides a 0–5 ppm O_2 atmosphere maintained by flowing 5% H_2 in N_2 gas over a Pd catalyst. We used DI water with an Eh range of −100 to −200 mV (average = −150 mV) measured using an ORP probe calibrated with an ORP standard (Eh = +420 mV). The low Eh of D.I. water was obtained by purging it with Ar and then leaving the bottle containing the water partly open in the anoxic hood for 3 days. To evaluate if a lower Eh impacted Ba release we also carried out one experiment with Eh < −300 mV. All vessels used in the experiments were made of Teflon and were cleaned by boiling in aqua-regia and then DI water. The vessels were then left inside the anoxic hood to equilibrate with the ambient atmosphere

for 24 h. The samples were placed in 60 mL leak-proof Savillex bombs. They were then heated to 80 °C and stirred with Teflon coated magnetic bar at 200 rpm. The reaction temperature within the bombs for the duration of the experiments is estimated to have remained at 80 ± 5 °C, as determined from repeated measurements of water using the same configuration as in the water-rock interaction experiments. Following the completion of an experiment, the water was filtered through disposable 0.25 μm nitrocellulose filter units. To prevent precipitation of barite which would compromise subsequent Ba determinations an aliquot of the sample solution was acidified with 20 μL HNO_3 per mL of sample within the anoxic chamber. This procedure eliminated the potential of Ba in solution combining with SO_4^{2-} to make insoluble barite during short-term storage prior to measurements.

2.2.5. ICP measurements

Major and trace elements (listed in Table 2) for all rock digestions, extractions and leaches were measured by ICPOES (Thermo Iris Intrepid 2); U was measured by quadrupole ICPMS (Agilent 7500c). As these solutions were comparable in major element composition to typical surface water, the synthetic water reference material NIST 1640a was used for quality control. All reported elements showed recoveries within 5% of accepted values of the reference material. Reported uncertainties represent propagated 2-sigma errors. Reported uncertainties are propagated formally according to the fundamental calculation:

$$C = k \cdot \frac{I_a - I_b}{I_{is}} \cdot S \quad (1)$$

where C is concentration [ug mL^{-1}], k is time-dependent drift monitored with a continuing verification standard, I_a is analyte count rate, I_b is time-dependent background count rate, I_{is} is matched internal standard count rate, S is sensitivity [ug mL^{-1}] derived from linear calibration. The low detection limits of ICPOES for Ba (<0.001 ug mL^{-1}) allow us to avoid spectral interferences and minimize sample matrix effects by measuring very dilute solutions. All extraction, leachate and digestion results are corrected for procedural blanks.

3. Results

3.1. Mineralogy

X-ray diffraction patterns confirm the presence of illite, quartz, calcite and pyrite in CC, YC and IC samples. Quantitative analysis using an internal standard method shows the CC sample has a mineralogical composition of 33% quartz, 31% illite, 16% chlorite, 15% calcite, 4% pyrite, and 1% barite; YC contains 36% illite, 33% quartz, 20% calcite, 9% pyrite and 2% chlorite; IC contains 39% illite, 36% quartz, 20% chlorite, 3% pyrite and 2% calcite. Note that the estimated error in analysis is approximately ±3 wt.%. No barite peaks are observed in the XRD patterns for YC and IC, indicating that the Ba content is lower than the XRD detection limits. No barite was observed in YC and IC samples with SEM. Barite is only observed in SEM micrographs for CC (Fig. 3) and is the only Ba-containing mineral phase present above the detection limits of EDS (~0.1 wt.%) in any of the samples. The barite in CC is contained within ellipsoid-shaped grains having a diameter of ~100 μm interspersed throughout the shale matrix (Fig. 3a). A majority of the barite grains are associated with pyrite (FeS_2) which exhibits various forms including cubic, finely-disseminated massive, framboidal, or a combination of massive and framboidal morphologies. Specifically, barite within the ellipsoid grains is often encapsulated within a pyrite matrix as shown in Fig. 3 micrograph and accompanying elemental maps for Fe (red) and Ba (blue). We suggest that authigenic barite was replaced by pyrite during early diagenesis based on sulfur isotope values and replacement textures exhibited by the barite-pyrite grains (see Niu et al. (2015 in review) for a detailed discussion).

The YC sample does not contain barite as shown in a representative micrograph and associated elemental maps for Ba and Fe in Fig. 4. Small grains (<1 μm) showing elevated Ba (grains highlighted in blue) were determined to be rutile, TiO_2, after closer inspection of the individual grains and a lack of correlation with S. The closeness of the Ba Lα line (E = 4.47 keV) and Ti Kα line (E = 4.51 keV) made it difficult to differentiate between the two elements in small grains. No barite was observed in micrographs for the IC sample (not shown).

Table 2
Whole-rock major and trace element data for selected Marcellus Shale core samples and reference materials.

	Chenango County	Yates County	Indiana County	SGR-1	SGR-1	SDO-1	SDO-1
	(n = 3)	(n = 1)	(n = 1)	(n = 3)	*Certified value*	(n = 2)	*certified value*
Al[a] (%)	7.4 ± 0.2	5.69 ± 0.12	9.3 ± 0.2	3.33 ± 0.09	3.45 ± 0.22	6.71 ± 0.20	6.49 ± 0.12
Fe[a] (%)	3.86 ± 0.11	4.15 ± 0.09	4.21 ± 0.08	2.08 ± 0.06	2.12 ± 0.20	6.29 ± 0.14	6.53 ± 0.15
Mn[a] (ug/g)	360 ± 11	40 ± 40	340 ± 70	244 ± 15	267 ± 68	297 ± 8	330 ± 40
Mg[a] (%)	0.80 ± 0.03	0.72 ± 0.03	1.14 ± 0.04	2.67 ± 0.07	2.68 ± 0.24	0.85 ± 0.04	0.93 ± 0.02
Ca[a] (%)	5.99 ± 0.10	6.96 ± 0.14	2.11 ± 0.04	5.85 ± 0.10	5.99 ± 0.24	0.74 ± 0.02	0.75 ± 0.03
Na[a] (%)	0.35 ± 0.01	0.17 ± 0.11	0.48 ± 0.10	2.21 ± 0.13	2.22 ± 0.20	0.26 ± 0.02	0.28 ± 0.05
K[a] (%)	2.60 ± 0.08	3.22 ± 0.17	3.7 ± 0.2	1.34 ± 0.07	1.38 ± 0.17	2.66 ± 0.08	2.78 ± 0.05
S[a] (%)	2.35 ± 0.05	4.39 ± 0.10	1.46 ± 0.03	1.52 ± 0.03	1.53 ± 0.22	5.4 ± 0.2	5.4 ± 0.9
P[a] (ug/g)	517 ± 33	600 ± 40	400 ± 50	1250 ± 50	1400 ± 600	470 ± 30	480 ± 30
Ba[a] (ug/g)	5000 ± 120	398 ± 8	752 ± 15	290 ± 20	290 ± 80	392 ± 8	400 ± 40
Sr[a] (ug/g)	261 ± 6	251 ± 11	245 ± 11	405 ± 15	420 ± 60	75 ± 2	75 ± 11
Mo[a] (ug/g)	80 ± 30	250 ± 20	26 ± 15	39 ± 12	35 ± 2	141 ± 6	130 ± 20
Ni[a] (ug/g)	103 ± 4	340 ± 20	74 ± 17	32 ± 16	29 ± 0	94 ± 2	100 ± 10
V[a] (ug/g)	208 ± 7	830 ± 30	180 ± 20	140 ± 20	130 ± 12	160 ± 6	160 ± 20
U[a] (ug/g)	13.5 ± 0.3	n/a	n/a	n/a	n/a	n/a	n/a
LOI[b] (%)	7.4	16.8	6.0	n/a	24.8	n/a	9.7 ± 0.5
Total carbonate[b] (%)	6.6	8.7	3.8	n/a	3.2	n/a	1.0 ± 0.20
Surface area[c] (m^2/g)	17	28	n/a	n/a	n/a	n/a	n/a
Particle size[d] (μm)	3.3 ± 3.4	2.7 ± 2.4	2.6 ± 2.8	n/a	n/a	n/a	n/a

[a] elemental measurements by ICP-OES, except U by ICPMS (n = 1), with 2σ propagated uncertainties.
[b] Loss-on-ignition assessed in triplicate with 0.5, 1.0 and 1.5 g samples. Mass loss measured following sequential combustion at 110 °C for 20 h, 550 °C for 102 h (LOI) and 990 °C for 24 h (carbonate as CO_2).
[c] Brunauer-Emmett-Teller (BET) single-point N_2 adsorption method.
[d] Pulverized shale median particle size (and 2σ standard deviation) by laser-scattering method with Fraunhofer optical model. n/a specifies data not available.

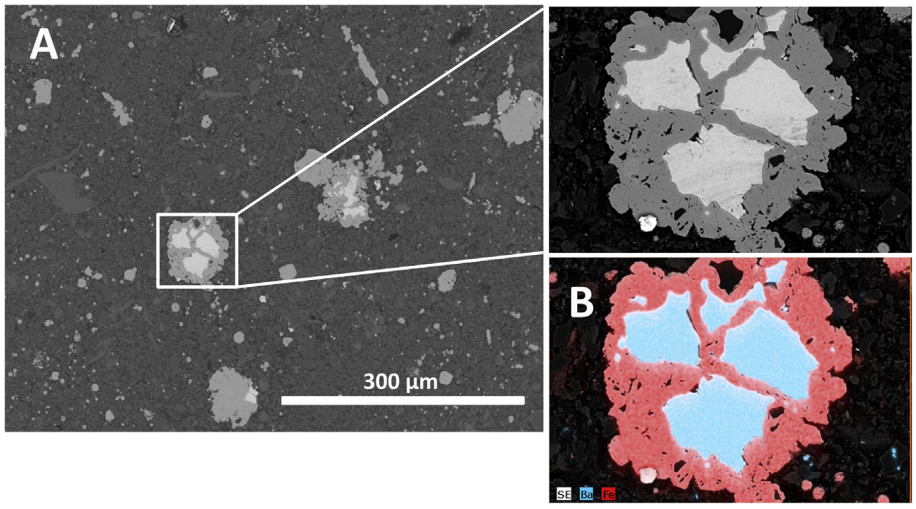

Fig. 3. Scanning electron micrograph and elemental maps for a representative area of the CC sample. A. Backscattered electron (BSE) image showing the shale matrix containing large barite-pyrite grains (inset). B. Elemental maps for Ba and Fe within large grain in inset.

3.2. Bulk rock composition

The whole rock composition including LOI and total carbonate for each sample is shown in Table 2 along with Green River Shale (SGR-1) and Devonian Ohio Shale (SDO-1) standards for comparison. All samples are organic-rich with LOI values between 6% and 18% which are consistent with rock units targeted for gas extraction (Wang and Carr, 2013). The total concentration of Ba in CC, YC, and IC is 5007 ± 121 µg/g, 398 ± 8 µg/g, and 752 ± 15 µg/g, respectively, based on averages of multiple chemical analyses. The concentration of Ba in the CC sample, the only sample containing barite, is an order of magnitude higher than the concentrations in YC and IC. The range of Ba concentration in these three samples provides a good representation of the range observed in MS (Lash and Blood, 2014; Werne et al., 2002). All samples are depleted in P (~0.05%) relative to SGR-1 and contain similar amounts of Sr (~250 mg/g). In terms of paleo-redox markers, we find that the YC sample contains the highest amounts of S, V and Mo (see Table 2). Indeed the YC sample has amongst the highest concentration of these elements measured within the MS (Werne et al., 2002).

3.3. Sequential extractions

Prior to discussing the insights gained from sequential leaching we first consider the issue of variable total yields for different elements. The sequential extraction procedure that we designed was intended to provide best characterization of each extraction rather than mass balance for the total procedure. Thus, we find that the total yield for elements other than Ca, while high, is not 100% (Table 3). For example, total Ba yields from sequential extractions are in the range of 84–91%. One possibility considered is that Ba is locked up in the residual refractory phases remaining at the end. In order to rule this out, we repeated steps F7 until no additional Ba was released and no visible residue remained. Moreover, total acid digestion in step F8 yielded no barium, and SEM/EDS analysis showed no Ba-containing solids in the residue. In addition, as Ba yields are similar to other elements measured such as Sr, Mg, and Fe (Table 3) an alternate explanation is needed to explain less than 100% for all these elements. Inspection of Table 3 shows that, 80–95% of Ca, whose yield is 100%, is removed in a single step (acetic acid leaching step, F3) whereas Ba, Sr, Mg, and Fe are incrementally leached out from the rocks. This suggests that incomplete yields are most likely attributable to minor incremental mass losses occurring over many sequential extraction steps (~40 individual steps) in which leachates are filtered at 0.2 um to remove particulates. As the accrued elements losses are 15% or less we assume for the following discussion that they do not impact our key conclusions.

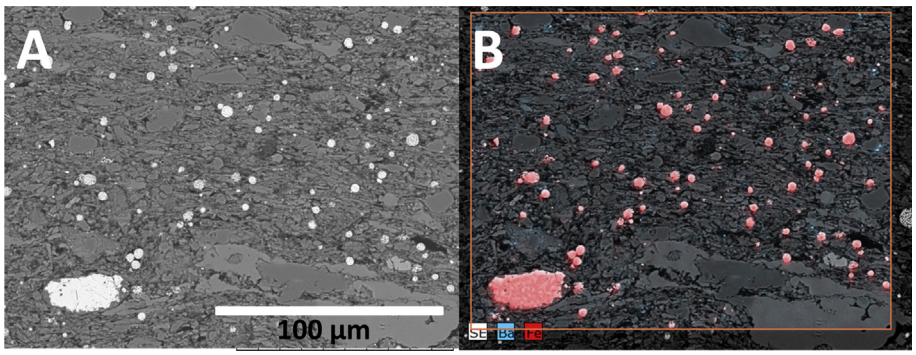

Fig. 4. Scanning electron micrograph and elemental maps for a representative area of the YC sample. A. BSE image of the clay-organic matrix with framboidal pyrites distributed throughout the section. A relatively-larger pyrite grain is present in bottom left of micrograph. No barite grains are observable in the micrograph. B. Elemental maps for Ba and Fe within the area of the micrograph. Small particles showing elevated Ba were shown to be due to overlap between Ti and Ba X-ray peaks; particles were determined to be rutile, TiO_2, after further inspection.

Table 3
Elemental yields from sequential extraction leachates (F1–F8) for CC, YC, and IC. Averages with 2σ standard deviations reported for replicates. All other values reported with 2σ analytical uncertainties. n/a specifies data not available, n/d specifies non-detectable.

Chenango County	Elemental yields (wt. %)						
Extraction	Ba	Sr	Ca	Fe	S	Na	Mg
DI H_2O (F1)	0.003 ± 0.002	2.1 ± 0.4	1.07 ± 0.04	0.003 ± 0.003	3.57 ± 0.13	14.8 ± 0.7	0.63 ± 0.04
$CaCl_2$ (F2)	2.37 ± 0.03	n/a	n/a	0.011 ± 0.005	0.87 ± 0.04	n/a	0.56 ± 0.04
Acet (F3)	0.44 ± 0.01	40.7 ± 1.8	95 ± 4	8.4 ± 0.3	0.69 ± 0.03	3.8 ± 0.3	17.7 ± 0.8
Perox (F4a + 4b)	4.64 ± 0.15	4.80 ± 0.15	2.60 ± 0.10	56.2 ± 1.2	85 ± 3	n/a	12.4 ± 0.4
Hydrox (f5)	0.66 ± 0.02	1.24 ± 0.13	0.01 ± 0.02	8.6 ± 0.3	0.43 ± 0.06	n/a	7.9 ± 0.5
HF (F6a + 6b)	55.3 ± 0.7	34.9 ± 0.5	0.18 ± 0.01	24.9 ± 0.3	2.72 ± 0.08	74.5 ± 1.9	57 ± 2
Carb (F7)	28 ± 1	7.9 ± 0.3	0.03 ± 0.01	0.23 ± 0.01	0.67 ± 0.05	n/a	n/a
Digest (F8)	0.99 ± 0.02	0.39 ± 0.01	0.012 ± 0.004	0.039 ± 0.002	0.08 ± 0.02	1.18 ± 0.12	0.03 ± 0.02
Sum	92.2 ± 1.3	92 ± 2	99 ± 4	98.4 ± 1.3	94 ± 3	94 ± 2	96 ± 2
Indiana County							
Extraction	**Ba**	**Sr**	**Ca**	**Fe**	**S**	**Na**	**Mg**
DI H_2O (F1)	0.06 ± 0.021	14.8 ± 0.8	9.5 ± 0.4	0.003 ± 0.002	14.9 ± 0.6	13.7 ± 0.9	1.75 ± 0.1
$CaCl_2$ (F2)	5.43 ± 0.10	n/a	n/a	0.008 ± 0.006	2.33 ± 0.07	n/a	1.38 ± 0.07
Acet (F3)	2.31 ± 0.05	43.3 ± 1.2	81 ± 2	14.2 ± 0.2	2.84 ± 0.08	5.1 ± 0.3	18.2 ± 0.8
Perox (F4a + 4b)	9.4 ± 0.6	16.8 ± 0.4	14.4 ± 0.5	20.9 ± 0.5	65 ± 2	n/a	8.1 ± 0.3
Hydrox (F5)	0.80 ± 0.09	0.56 ± 0.14	0.10 ± 0.03	18.8 ± 0.7	4.1 ± 0.2	n/a	8.3 ± 0.5
HF (F6a + 6b)	69.4 ± 0.7	16.6 ± 0.4	0.52 ± 0.03	40.7 ± 0.5	2.94 ± 0.13	74 ± 2	54 ± 2
Carb (F7)	0.08 ± 0.02	0.02 ± 0.01	0.06 ± 0.02	0.23 ± 0.01	n/d	n/a	n/a
Digest (F8)	0.05 ± 0.02	0.05 ± 0.01	0.04 ± 0.01	0.012 ± 0.004	0.05 ± 0.08	0.10 ± 0.07	0.04 ± 0.01
Sum	88 ± 1	92 ± 2	105 ± 2	94.8 ± 1.1	92 ± 2	93 ± 2	92 ± 2
Yates County							
Extraction	**Ba**	**Sr**	**Ca**	**Fe**	**S**	**Na**	**Mg**
DI H_2O (F1)	0.11 ± 0.02	3.6 ± 0.9	2.34 ± 0.06	0.001 ± 0.002	3.80 ± 0.08	16 ± 2	1.17 ± 0.07
$CaCl_2$ (F2)	4.18 ± 0.08	n/a	n/a	0.010 ± 0.005	0.70 ± 0.02	n/a	0.89 ± 0.07
Acet (F3)	2.99 ± 0.07	68 ± 2	91 ± 2	3.23 ± 0.05	1.09 ± 0.03	7.9 ± 0.8	22 ± 1
Perox (F4a + 4b)	6.5 ± 0.3	10.1 ± 0.3	7.5 ± 0.3	82 ± 2	89 ± 3	n/a	8.5 ± 0.4
Hydrox (F5)	0.79 ± 0.14	0.02 ± 0.10	0.01 ± 0.01	0.44 ± 0.02	0.10 ± 0.03	n/a	0.95 ± 0.13
HF (F6a + 6b)	77 ± 1	7.8 ± 0.1	0.16 ± 0.01	9.6 ± 0.2	0.17 ± 0.04	88 ± 7	55 ± 2
Carb (F7)	0.11 ± 0.03	0.04 ± 0.02	0.016 ± 0.005	0.26 ± 0.01	n/d	n/a	n/a
Digest (F8)	0.04 ± 0.03	0.08 ± 0.02	0.013 ± 0.004	0.009 ± 0.002	0.005 ± 0.012	0.5 ± 0.2	n/d
Sum	91.2 ± 1.0	90 ± 2	101 ± 2	96 ± 2	95 ± 3	113 ± 7	90 ± 3

Table 3 summarizes the sequential extraction conditions and elemental yields (x = Ba, Sr, Ca, Fe and S) in the leachate from each extraction step. Elemental yields are determined by:

$$\%\ yield(element\ x) = \left[\frac{moles(x)\ in\ leachate}{moles(x)\ in\ rock}\right] \times 100 \qquad (2)$$

For all samples, a majority of the Ba in the rock (55–77%) leaches out in two steps: the HF extraction (F6a) for the silicate dissolvable fraction and the $AlCl_3$ rinse (F6b) to remove insoluble fluoride salts formed in F6. The cumulative Ba yield for all prior steps (*i.e.*, F1 through F5) is 8% (CC), 14% (YC), and 19% (IC). For CC only, 20% of the total Ba is extracted in the Curie carbonate extraction for the barite dissolvable fraction (F7) consistent with the presence of barite grains in micrographs (Fig. 2). SEM analysis of the solids remaining after the F8 leachate is removed show only rutile, zircon, metal oxide phases, and highly refractory C. All of the barite appears to be removed in the F7 extraction. Both YC and IC samples show negligible barium in F7 leachate consistent with the lack of any observable barite in micrographs.

3.4. X-ray fluorescence spectrometry (μ-XRF)

Sequential extraction results suggest that approximately 55–77% of the Ba is associated with the dissolvable silicate fraction in the shale. To confirm the association of Ba with silicate minerals, we evaluated the spatial distribution and elemental correlations of Ba, Si, Al, Fe and S within thin sections of the CC sample. Elemental maps of Si and Al are shown in Fig. 5. The spatial correlation between Al and Si shows the distribution of clays and fine particles of quartz in the section. The elemental map of Ba is shown for the Ba Lβ_2 line ($E_{X\text{-}ray}$ = 5.15 keV) instead of the Ba Lα (E = 4.47 keV) to avoid false positive signals due to an overlap with the Ti Kα line (E = 4.51 keV). This is required due to the presence of fine particles of TiO_2 that appear in micrographs of the same section. Discrete grains of barite previously identified in SEM micrographs in both the calcite vein and silicate-clay matrix appear as bright areas in the Ba map and spatially correlate with S. Sulfur associated with barite is less intense than S from pyrite (Fig. 5) due to the large difference in S concentration between the two minerals, 13.7 wt.% vs. 53.5 wt.%, respectively. The brightest areas in the S map correspond to pyrite grains as shown by comparing the S and Fe maps. Barite and pyrite are often closely associated with each other in the CC sample. In addition to discrete grains or grains associated with pyrite, elevated levels of Ba are spatially associated with clays as shown by the diffuse Ba signal within the clay matrix, which is intense relative to that within the calcite vein.

3.5. Anoxic leaching experiments

Table 3 summarizes the leaching solution conditions and the Ba and S concentrations in the leachate from each experiment as well as the percentage of Ba that dissolves into the leachate from the rock (i.e. Ba yield). The Ba yield is determined by Eqn. (2). Figs. 6 and 7 graphically summarize the leaching results for Ba and S from CC

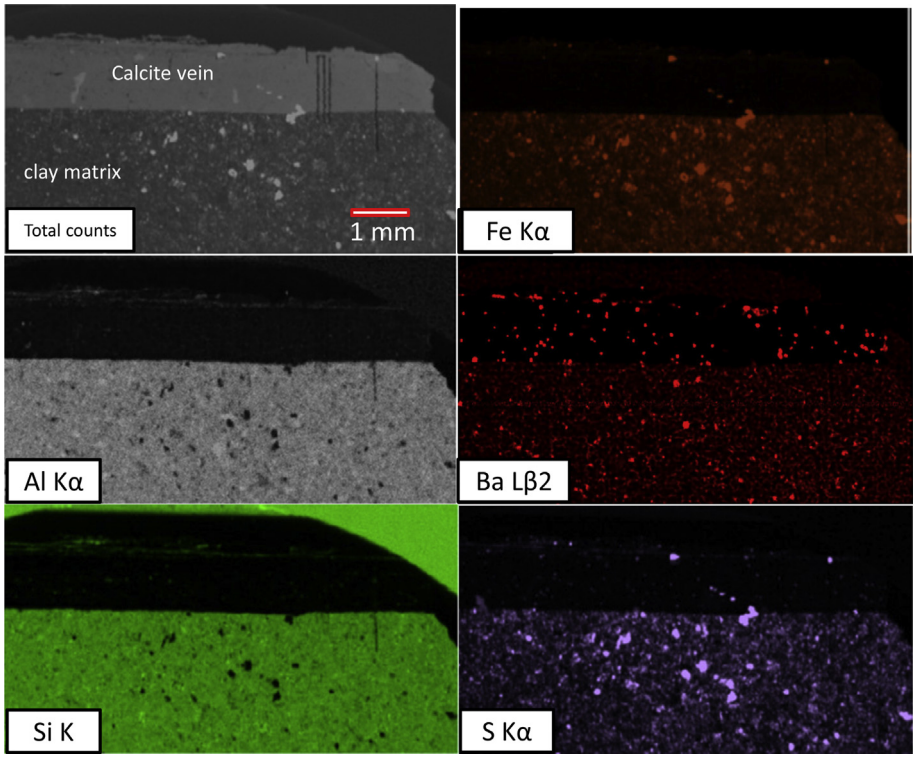

Fig. 5. Elemental maps of a representative area of the CC sample obtained by μ-XRF analysis. Top left image is total X-ray counts for clay-organic matrix contiguous with a calcite vein in the section. Elemental maps (total counts) are shown for Fe(Kα), Al(Kα), Ba(Lβ2), Si(Kα) and S(Kα).

and YC, respectively. The *x*-axis is normalized by the Ba:S ratio in the original rock to account for different Ba:S ratios between the original CC (Ba:S = 0.052) and YC (Ba:S = 0.022) samples prior to leaching experiments. The *y*-axis shows the concentration of Ba in solution after leaching as well as the Ba yield. The amount of Ba that dissolves into the leaching solutions increases with increasing ionic strength. Moreover, for a given ionic strength and duration of leaching the Ba yield from leaching using solutions containing only Ca^{2+} appears to be roughly two times that using solutions containing Na^{+}. Finally, changing Eh of the solutions from −150 mV to < −300 mV does not appear to substantially change the Ba yields (Fig. 6).

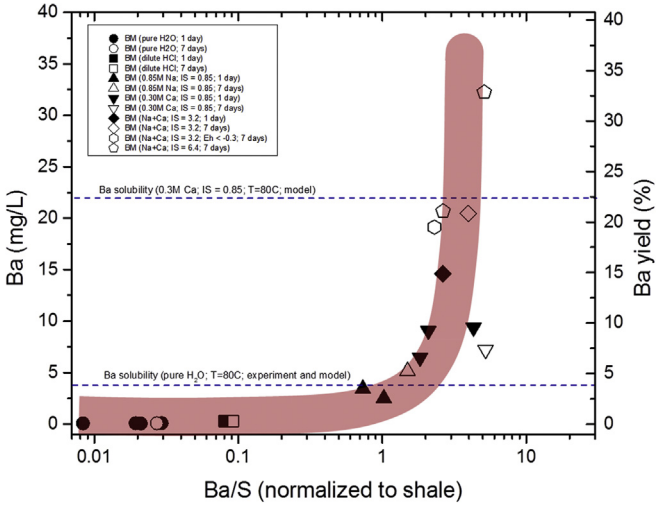

Fig. 6. Ba yield in leachate versus the Ba/S ratio for CC. The *x*-axis is normalized by the Ba:S ratio in the original rock (Ba:S = 0.052) to account for different Ba:S ratios between the samples prior to leaching experiments. The *y*-axis shows the concentration of Ba in solution after leaching as well as the Ba yield. Solid and open symbols represent 1 day and 7 day leaching experiments, respectively. Shaded region roughly shows upward trend in yield with increasing Ba/S ratio and increasing ionic strength.

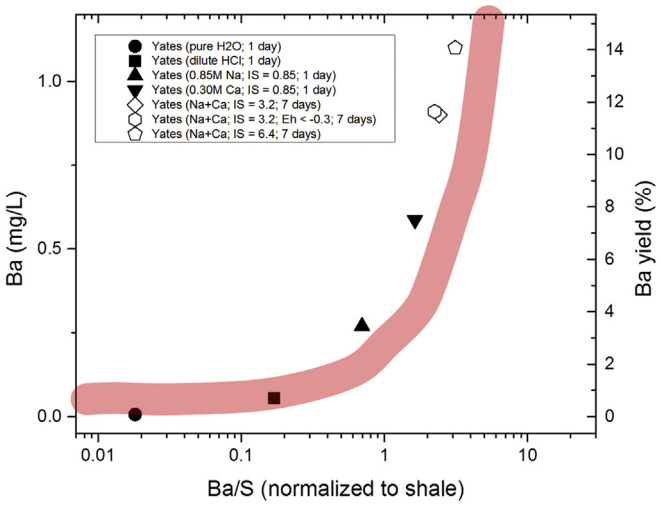

Fig. 7. Ba yield in leachate versus the Ba/S ratio for YC. The *x*-axis is normalized by the Ba:S ratio in the original rock (Ba:S = 0.022) to account for different Ba:S ratios between the samples prior to leaching experiments. The *y*-axis shows the concentration of Ba in solution after leaching as well as the Ba yield. Solid and open symbols represent 1 day and 7 day leaching experiments, respectively. Shaded region roughly shows upward trend in yield with increasing Ba/S ratio and increasing ionic strength.

4. Discussion

Mineralogical and sequential extraction results indicate that >55% of the total Ba in all samples is strongly partitioned into clays. Moreover, experiments simulating water-rock interaction show that between 5 and 25% of the total Ba barium is released from the rock in high ionic strength solutions. We discuss below the results of the sequential leaching experiments and examine possible mechanisms that allow clays to sequester Ba. We then discuss the results of simulated water-rock reactions during hydraulic fracturing and investigate the extent to which Ba associated with the cation-exchangeable fraction is released during hydraulic fracturing. Finally, we estimate water to rock ratios using a number of major elements in the wastewater and discuss the potential role that scaling plays in controlling their concentrations.

4.1. Sequential leaching and Ba reservoirs within Marcellus Shale

For all samples, <20% of the total Ba in the rock is extracted in the F1–F5 steps after accounting for Ba associated with the silicate fraction, Ba in barite (CC only), and the overall Ba yield for all sequential extraction steps. For all samples, a negligible amount of Ba is extracted in the F1 step indicating that Ba is not present as a water-soluble salt in the rock, despite the presence of significant Ca, Sr, Na, Mg, and S in F1 leachate (Table 3). Elements in F1 leachate are derived from dissolution of sulfate salts, or possibly chloride and/or bromide salts. We did not analyze for chloride or bromide in this study, but SEM/EDS analysis did confirm the presence of NaCl crystals exhibiting dendritic morphologies in the samples (Fig. 8). However, it should be noted that the halite crystals shown in Fig. 8 are extremely rare in the samples. The source of these salt crystals may be dried residues from Appalachian brine that is originally present as either free brine or capillary-bound water in the fine pores of the rock (Blauch et al., 2009; Capo et al., 2014; Dresel and Rose, 2010; Warner et al., 2012) and implicated as a source of TDS in produced water (Balashov et al., 2015; Chapman et al., 2012; Engle and Rowan, 2014).

However, Stewart et al. (2015) argue against dissolution of water-soluble components being the main source of high salinity in Marcellus produced waters by asserting that if Na, Ca, and Sr behave conservatively, the ratios of Na/Ca and Sr/Ca from experimental leachates of MS should be similar to the ratios determined from produced waters. The metal ratios reported in Stewart et al. (2015) are significantly lower than the range for produced waters suggesting that another source of TDS is required (Capo et al., 2014; Chapman et al., 2012; Haluszczak et al., 2013; Kohl et al., 2014). In our study, the ratio of Na/Ca and Sr/Ca averaged from F1 (water soluble fraction) is 0.78 and 0.0051, respectively, and are also lower than produced water ratios reported in the previous studies. Assuming that Na, Ca, and Sr behave conservatively, our results are consistent with Stewart et al. (2015) in suggesting that produced water Na, Ca and Sr compositions may derive, in part, from the mixing of formation water with injected fluids. However, this interpretation should be made with the understanding that Ca and Sr may not behave conservatively in produced water due to the possibility of carbonate and sulfate scale formation (EPA, 2011; Gregory et al., 2011; Vidic et al., 2013) and discussed in section 4.4.

With respect to barium in produced water, Stewart et al. (2015) report significant overlap between Ba/Ca values in water soluble and cation-exchangeable leachates and those of produced waters, but assert that overlap may be due to the wide range of Ba/Ca in produced waters resulting from differences in the extent of barite scale formation or variations in sulfate levels between different well sites (Engle and Rowan, 2014). Variability in Ba/Ca may also be explained by the extreme variability in cation-exchangeable Ba shown from leaching experiments in this study and previous studies (Phan et al., 2015; Stewart et al., 2015). Thus, Ba/Ca does not rule out the possibility that water-rock interactions are a source of Ba in produced water.

For the samples in this study, an extremely small amount of Ba is released when rock mixes with pure water (Ba/Ca = 9.5×10^{-5}) suggesting that either: 1) Ba is not present in the original brine (or dried salt residue left in the rock), 2) these samples do not contain original brine (or dried salts), or 3) Ba and S present in brine forms relatively insoluble barite when the rock is exposed to oxidizing conditions. The latter would occur when the core rock is extracted and brought to the surface, and could contribute to additional Ba measured in sequential extractions steps F1–F6. If so, any barite formed in this manner has been completed removed by steps F1–F6 as shown from the negligible Ba in step F7 of the YC and IC extractions.

For CC, YC, and IC samples, approximately 2.4%, 4.2%, and 5.4% of the total Ba, respectively, is released as a cation-exchangeable fraction in 1 M $CaCl_2$ (F2). However, assessing Ba speciation from F2–F5 steps is not straightforward for rocks containing barite (e.g., CC in this study). For CC, operational definitions breakdown when the leaching media has a high ionic strength. For example, Ba can be leached from CC in a 1 M $CaCl_2$ solution (F2) due to: 1) isovalent Ca^{2+} exchange with Ba^{2+} from clay and, 2) increased solubility and accelerated dissolution kinetics of barite under high ionic strength conditions as described in previous studies (Blount, 1977; Kowacz and Putnis, 2008; Monnin, 1995, 1999; Monnin and Galinier, 1988; Risthaus et al., 2001). For CC, most of the Ba (~70%) from the F2 extraction step comes out in the first of the four extraction steps. The Ba concentration in the first leachate is 90 μg/g, which is ~3 × greater than the Ba concentration predicted based on the solubility of barite under similar conditions (32 μg/g). The comparison suggests that most of the Ba in F2 is coming from the clay exchangeable fraction. However, the possibility of some amount of Ba release from barite must be considered at these high ionic strengths (IS = 3). It is to be noted that due to the high ionic strength of the solution we consider it more likely that barite will dissolve and not precipitate (see more on this in the next section).

The acetic acid (F3) and peroxide (F4) steps are operationally-defined to extract Ba associated with carbonate and organic phases, respectively, but these steps may also expose Ba-containing phases (e.g., clays and barite) that were inaccessible to the extraction solution in the previous steps. It is possible that Ba phases may

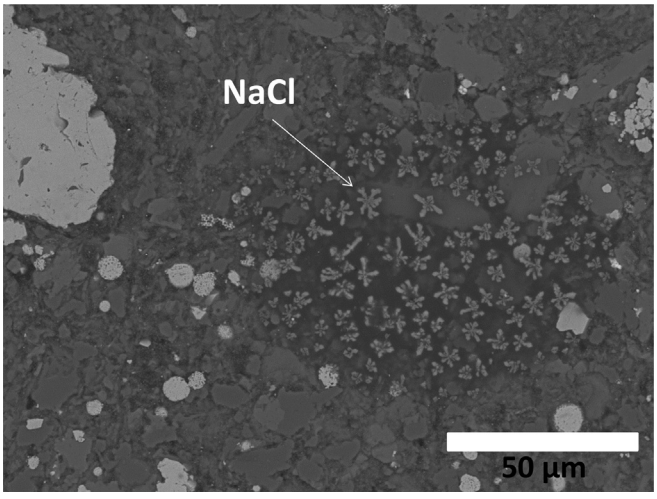

Fig. 8. Scanning electron micrograph of the YC sample showing dendritic NaCl crystals concentrated within a small area within the section.

be buried within the clay-organic-carbonate aggregates that constitute the powdered samples and are only exposed (and thus able to release Ba) after carbonates and clays are dissolved in F3 and F4.

Though CC contains observable barite, results shown in Table 3 indicate that a majority (~55%) of the total Ba in CC is extracted in the $F6_{(a\text{-}b)}$ (*i.e.*, HF + $AlCl_3$) steps, which are designed to dissolve silicates. The sum of $F6_{(a\text{-}b)}$ is operationally defined to include all Ba strongly bound to or structurally-incorporated into silicate minerals. For YC and IC, the percentage of total Ba coming out in $F6_{(a\text{-}b)}$ is ~76% and ~69%, respectively. This result and the positive correlation between Ba and Al shown in μ-XRF elemental maps (Fig. 5) indicate that the majority of Ba in the in the shale is associated with clay minerals, or illites as indicated from XRD of CC. The fact that the majority of Ba is released only after silicates are dissolved by HF suggests that a majority of Ba is either strongly bound to clay interlayers or incorporated into the phyllosilicate structure itself. It is interesting to note that despite the abundance of diagenetic barite grains in CC from micrographs, only ~20% of the total Ba was extracted in the carbonate extraction step (F7). Negligible Ba in the F7 fraction of YC and IC suggests that there is minimal secondary barite formation by precipitation of Ba and SO_4^{2-} leached in F1–F6 extractions. This is an important observation because quantifying the fraction of barite barium would be compromised if barite were precipitating during prior extraction steps.

In summary, evaluation of mineralogy combined with sequential extraction lead us to the following conclusions: 1) Despite the presence of authigenic barite crystals in CC, only ~20% of total Ba is actually contained in the barite phase; negligible barite is found in YC and IC samples. 2) Negligible Ba is released in pure H_2O suggesting that dried brine residues, or salts, *per se* may not be a source of Ba in these rocks. 3) Approximately 8% (CC), 18% (IC), and 15% (YC) of the total Ba is released from the rock in extraction steps F2–F5 and these should be considered an upper limit of the extent to which Ba is associated with phases that are leachable during hydraulic fracturing (e.g., soluble salts, exchangeable sites on clays, carbonates, or organics). 4) Significantly, the majority of Ba in *all* samples is associated with clay minerals and is only leached from the rock after treatment in strong HF acid.

4.1.1. Barium incorporation into phyllosilicate minerals

The key issue we examine next is when and how is Ba being introduced into clays. Could Ba be present in the original detrital clays comprising the MS? Direct observations of the behavior of Ba in estuaries and experimental studies have demonstrated that the adsorption efficiency of Ba^{2+} for clays decreases significantly as the ionic strength of the water increases (Atun and Bascetin, 2003; Coffey et al., 1997; Zhang et al., 2001). These results point out that any Ba^{2+} adsorbed on detrital clays will likely be released in the high ionic strength marine environment. Direct observations of sediment traps and recent marine sediments indicate, however, that detrital clays contain on average about 400 μg/g of Ba (Dymond et al., 1992; Gingele and Dahmke, 1994; Klump et al., 2000; Pirrung et al., 2008). These observations suggest that a substantial amount of Ba in detrital clays is not removed in marine environment and is likely present as a structural component of the clays.

Hosterman and Whitlow (1983) reports that the clay fraction from samples of MS across the basin consists mainly of authigenic illite, smectite-illite mixed clays and chlorite that were formed during early diagenesis/low grade metamorphism of terrigenous (detrital or volcanic) smectitic clays. The authigenic clays are produced as a result of the following reaction as described by Hosterman and Whitlow (1983): smectite + potassium feldspar → illite + chlorite + quartz. Since most of the Ba in the shale is in a HF-dissolvable silicate fraction rather than in the exchangeable fraction, the above observation would suggest that Ba associated with terrigenous smectites was preferentially partitioned into or retained by authigenic clays during early diagenesis/low grade metamorphism. Finally, if authigenic barite is dissolved during the conversion of smectite to illite and chlorite, it could also be a source Ba to the new clays. It is, at present, unclear as to how processes that affect the diagenesis of clays (e.g., smectite to illite conversion) will also affect the structural position of Ba within clays. Phan et al. (2015) reports upwards of 75% cation-exchangeable Ba in dry-drilled MS cuttings that are depleted in Ba relative to the 580 ppm crustal average for shale (Wedepohl, 1971)) and contain <1 wt.% TOC. This result, along with the extreme variability in cation-exchangeable Ba reported for all of their MS samples (9–74% of total Ba), suggests that diagenetic processes that allow partitioning of Ba in these clays are not understood and should be an area of future study.

4.2. Hydraulic fracturing and reductive weathering of Marcellus Shale

Our experiments emulating water-rock interactions during hydraulic fracturing show that at elevated temperatures, high pH and under anoxic conditions powdered MS releases significant quantities of elements, which possibly involve hydrothermal breakdown of hydrocarbons, release of sulfur, dissolution of carbonates and other salts, and cation exchange reactions with clays. These 'reductive weathering' reactions are fundamentally different from oxidative weathering reactions occurring at the earth's surface, which are characterized by production of sulfuric and carbonic acids via breakdown of sulfides and hydrocarbons and dissolution of carbonates (Farquhar et al., 2000), and leaching of aluminosilicates by low pH solutions (Cronan and Schofield, 1979). In this study, we confine our attention to the reductive weathering mechanisms involved in the release of Ba from black shale.

Leaching experiments done in DI H_2O and dilute HCl (0.1 M) provide baseline values for Ba yields. After immersion in anoxic H_2O for 1 day, the CC and YC samples lose less than 0.1% of the total Ba into the leachate (see Table 4) which is likely sourced from relatively soluble salts or Ba that is weakly-bound to mineral surfaces consistent with leachate from F1 step in sequential extractions. There is no significant increase in Ba yield from day 1 to day 7 as shown by CC in Table 4. It should be noted that if Ba concentrations are controlled by dissolution of barite in the CC sample, for example, then approximately 4% of the total Ba is expected to leach from the rock based on the known solubility of barite ($T = 80\ ^\circ C$ (Blount, 1977)). It is most likely that the barite dissolution rate in pure H_2O is too slow even under elevated temperatures for barium to reach the solubility limit in 7 days. It is also reasonable to assume that, under low ionic strength conditions, some amount of Ba dissolving from barite may sorb to clays in the sample. For example, Atun and Bascetin (2003) show that Ba sorption to clays is low at ionic strength >0.1, but at the lowest ionic strength of their study (~0.003 M) illite clays can sorb between 45 and 60% of Ba in solution.

Less than 1% of the total Ba was leached from the samples during treatment in 0.1 M HCl solution, which is expected to dissolve most of the acid-soluble carbonates. This result is consistent with a lack of correlation between Ba and Ca in elemental maps (Fig. 5). For example, Ba within the calcite vein (shown in Fig. 5) is contained within discrete barite and barite-pyrite grains and not distributed within the calcite matrix. In addition, a laser ablation ICPMS transect across the same calcite vein (transect not shown) showed no correlation between Ca and Ba.

Barium is only released from the rock in significant quantities when the ionic strength of the leaching solution is high. At an

Table 4
Elemental yields in simulated fracking leachate for CC and YC whole rock powders. Averages with 2σ standard deviations reported for replicates (n). All other values reported with 2σ analytical uncertainties. H_2O:shale weight ratio = 50:1. All experiments conducted in a Coy anaerobic glovebox. Please note that these yields are not cumulative in comparison to Table 3 n/a specifies data not available.

Leaching conditions		Ba (mg/L)	Elemental yields (wt. %)						
			Ba	Sr	Ca	Fe	S	Na	Mg
Chenango County									
DI H_2O; 1 day	(n = 4)	0.09 ± 0.02	0.09 ± 0.02	6.8 ± 0.8	2.1 ± 0.6	0.004 ± 0.003	3.9 ± 0.6	19 ± 3	1 ± 3
DI H_2O; 7 days	(n = 1)	0.094 ± 0.003	0.100 ± 0.004	8.0 ± 0.7	2.54 ± 0.08	0.006 ± 0.001	3.27 ± 0.11	19 ± 2	1.26 ± 0.07
Dilute HCl; 1 day	(n = 1)	0.281 ± 0.002	0.29 ± 0.01	26 ± 2	43 ± 1	1.38 ± 0.07	3.31 ± 0.11	19 ± 2	4.4 ± 0.3
Dilute HCl; 7 days	(n = 1)	0.298 ± 0.004	0.30 ± 0.01	26 ± 2	45 ± 1	0.68 ± 0.03	3.06 ± 0.09	19 ± 2	5.0 ± 0.3
0.85 M Na; IS = 0.85; 1 day	(n = 2)	2.9 ± 0.6	3.0 ± 0.5	17.2 ± 1.4	4.0 ± 0.5	0.005 ± 0.005	3.9 ± 0.8	n/a	1.7 ± 0.3
0.85 M Na; IS = 0.85; 7 days	(n = 1)	4.9 ± 0.2	5.0 ± 0.3	20 ± 2	5.9 ± 0.2	0.006 ± 0.001	4.22 ± 0.13	n/a	2.5 ± 0.2
0.30 M Ca; IS = 0.85; 1 day	(n = 3)	8.2 ± 1.3	8.4 ± 1.4	n/a	n/a	0.25 ± 0.09	4.2 ± 0.5	19 ± 6	7.2 ± 0.5
0.30 M Ca; IS = 0.85; 7 days	(n = 1)	7.1 ± 0.20	7.2 ± 0.3	n/a	n/a	0.60 ± 0.03	3.54 ± 0.10	17 ± 3	13.2 ± 0.8
Na + Ca; IS = 3.2; 1 day	(n = 1)	13.3 ± 0.2	13.5 ± 0.5	n/a	n/a	0.13 ± 0.01	4.76 ± 0.14	n/a	6.9 ± 0.4
Na + Ca; IS = 3.2; 7 days	(n = 1)	19.7 ± 0.6	20.1 ± 0.9	n/a	n/a	0.16 ± 0.01	4.35 ± 0.13	n/a	12.9 ± 0.8
Na + Ca; IS = 3.2; Eh < −0.3; 7 days	(n = 1)	18.6 ± 0.4	18.7 ± 0.10	n/a	n/a	n/a	6.5 ± 0.2	n/a	n/a
Na + Ca; IS = 6.4; 7 days	(n = 2)	26 ± 6	26 ± 6	n/a	n/a	n/a	5.6 ± 1.0	n/a	n/a
Yates County									
DI H_2O; 1 day	(n = 1)	0.006 ± 0.001	0.080 ± 0.001	7.8 ± 0.4	3.31 ± 0.07	0.01 ± 0.01	4.24 ± 0.10	21 ± 5	2.09 ± 0.09
DI H_2O; 7 days		n/a	n/a	n/a	n/a	n/a	n/a	n/a	n/a
Dilute HCl; 1 day	(n = 1)	0.054 ± 0.001	0.70 ± 0.01	35.6 ± 1.6	34.9 ± 0.7	0.62 ± 0.01	3.85 ± 0.09	23 ± 5	5.0 ± 0.2
Dilute HCl; 7 days		n/a	n/a	n/a	n/a	n/a	n/a	n/a	n/a
0.85 M Na; IS = 0.85; 1 day	(n = 1)	0.272 ± 0.005	3.58 ± 0.07	22.7 ± 1.0	6.35 ± 0.14	0.05 ± 0.01	4.63 ± 0.11	n/a	5.4 ± 0.3
0.85 M Na; IS = 0.85; 7 days		n/a	n/a	n/a	n/a	n/a	n/a	n/a	n/a
0.30 M Ca; IS = 0.85; 1 day	(n = 1)	0.547 ± 0.001	7.03 ± 0.13	n/a	n/a	0.08 ± 0.01	4.16 ± 0.10	31 ± 9	9.1 ± 0.4
0.30 M Ca; IS = 0.85; 7 days		n/a	n/a	n/a	n/a	n/a	n/a	n/a	n/a
Na + Ca; IS = 3.2; 1 day		n/a	n/a	n/a	n/a	n/a	n/a	n/a	n/a
Na + Ca; IS = 3.2; 7 days	(n = 1)	0.93 ± 0.02	11.9 ± 0.3	n/a	n/a	0.55 ± 0.01	4.48 ± 0.11	n/a	13.2 ± 0.6
Na + Ca; IS = 3.2; Eh < −0.3; 7 days	(n = 1)	0.89 ± 0.02	11.4 ± 0.1	n/a	n/a	n/a	4.85 ± 0.12	n/a	n/a
Na + Ca; IS = 6.4; 7 days	(n = 1)	0.90 ± 0.07	14.1 ± 0.9	n/a	n/a	n/a	3.68 ± 0.09	n/a	n/a

IS > 3.2, Ba yield is three to four orders of magnitude higher than in DI H_2O or dilute HCl as shown in Table 4. The positive correlation between the amount of Ba released from the rock and the ionic strength of the reacting medium (See Table 4 and Figs. 6–7) is consistent with the reported trends in produced water concentrations (Chapman et al., 2012; Rowan et al., 2015). An important conclusion to be drawn from the results summarized in Table 4 is that significant quantities of Ba are leached directly from the rock under anoxic and high ionic strength conditions in a timeframe relevant to the accumulation of Ba in produced waters. We thus propose that direct leaching from the host rock should be treated as a source of Ba in produced water, in addition to any Ba that may derive from the dilution of basinal brines by injected fluid.

The exact reaction mechanism for direct leaching is unclear, however the upward trends of the amount of Ba leached with respect to the Ba/S ratio for CC and YC are nearly identical (shown by the drawn-in shaded region in Figs. 6 and 7), which suggests that leaching occurs via similar processes in these two samples despite CC having an order of magnitude higher Ba concentration than YC, and the presence of barite in CC only. Further insight into the mechanism is revealed by the Ba yield being approximately 2 × higher for leaching experiments in solutions containing only Ca^{2+} versus those containing only Na^{+} (at equivalent ionic strength, IS = 0.85). This behavior is consistent with a cation exchange mechanism occurring on clay surfaces because isovalent exchange of 1 × Ca^{2+} for 1 × Ba^{2+} is more energetically favorable than 2 × Na^{+} exchanging with 1 × Ba^{2+}(Zhu, 2004). In making this assessment, we have also considered that the solubility of barite is equivalent in solutions containing only Ca or Na at equivalent ionic strength (Monnin and Galinier, 1988).

The highest Ba yields, 26.2 ± 6% (CC) and 14.1 ± 0.9% (YC), were obtained by leaching the rock in solutions with IS = 6.4 for 7 days (Table 4). In one particular experiment (IS = 6.4; 7 days), 33% of the Ba was leached from CC (see Fig. 6). It should be noted that the concentrations of Na and Ca at this ionic strength are at the upper limit for water-rock interactions in Marcellus wells based on produced water chemistry, but consistent with levels reported for Appalachian brines (Dresel and Rose, 2010). In general, approximately 5–25% of the total Ba in the rock is leached within 7 days under low Eh (between −100 and −200 mV), T = 80 °C, and salinities comparable to those reported for produced waters from Marcellus wells. In each case, the majority of the Ba is released within the first day of leaching. Barium yields for CC were generally higher than for YC and this may be due to dissolution of barite under high ionic strength conditions. An alternative explanation is that there is a larger fraction of more easily exchangeable Ba in the CC clays. Overall, the results of anoxic leaching are consistent with results from sequential extractions that show ~75% of total Ba in both CC and YC is locked up in relatively insoluble phases (e.g., silicate clays or silicate clays + barite) and unavailable to dissolution under the conditions of this study.

4.3. *Integrating multiple mechanisms in the generation of Marcellus brine composition*

Previous interpretations of Marcellus produced water provenance have focused on a binary mixing regime between dilute injectate and pre-existing basinal brines. We emphasize here that a variety of mechanisms are likely to contribute to the generation of produced water composition. The schematic in Fig. 1 summarizes possible mechanisms (designated 1–8) that control cation chemistry in produced water. Correlation between Ba and dissolved solids is typically explained by the mixing of Na- and Ca-rich basinal brines containing Ba with injected fluids of varying composition (1). Mixing is proposed to occur when (2) hydraulic fractures crosscut pre-existing fractures containing free brine or (3) porous lenses of silt, sand, or organics. However, free brine in MS is thought to be very minimal as suggested by well logs and other observations (Engelder, 2012; Engelder et al., 2014). Another possible mechanism (4) involves the diffusion of leachable ions

from rock matrix pores into hydrofractures containing injected fluid that are supported by proppant sand (Balashov et al., 2015). Dissolution of soluble salts (5) has also been invoked by Blauch et al. (2009) to explain high produced water TDS, as well as by Rowan et al. (2015) to balance Na–Br mixing that cannot be explained by pre-existing brines alone. Significant yields of Na and Ca in the anoxic DI H_2O leachate of our samples (Table 4) suggest that some form of brines (capillary bound) or dried brine residues are widely dispersed in shale. However, the low yields of Ba in the anoxic DI H_2O leachates of CC and YC indicate that brines may be a relatively minor source of Ba in these samples.

Here we posit a mechanism by which Ba is liberated from clays (6) due to ion exchange with Na and Ca that is driven by their ingrowth during hydraulic fracturing. The water-rock interaction is facilitated by the large surface area generated in the host formation by (7) small-scale fracturing and the production of fines (Bazant et al., 2014); which are also evident from the presence of clays in the 'impoundment sludge' that forms after the settling of fines from produced waters (Zhang et al., 2015b). We do not discount the possibility that brines in MS contain some amount of Ba that is contributing to Ba enrichment in produced water flowing back to the surface. Barium supplied by brine or by recycled injected water will not affect the partitioning of Ba from clay surfaces into produced water due to the overwhelming TDS levels. Sulfides present in the anoxic brine may oxidize to sulfate when the core rock is brought to the surface, causing any Ba that is present to precipitate as relatively-insoluble barite.

4.4. Quantitative constraints on water-rock interaction during hydraulic fracturing

As we have shown by the large amount of Ba and other cations readily leached from MS in relatively short time scales, the elevated elemental concentrations of produced water might be explained by the interaction between injection fluid and MS. Such a comparison fundamentally relies on knowledge of the water-to-rock ratio achieved during hydraulic fracturing, that is, the efficacy for a limited volume of injected fluid to interact with the fractured shale. Since the produced water elemental concentrations are far greater than the surface water it can be readily assumed that *W/R* ratio is quite low. A quantitative assessment can be obtained as follows. The concentration of an element in produced water resulting from the extraction of the element from a mass of rock (*R*) in a volume of what was originally surface water (*W*) used for hydraulic fracturing is:

$$WC_{mix} = WC_W + RC_R \tag{3}$$

where *C* is the concentration of the element and subscripts *mix*, *R* and *W* respectively denote, produced water, rock and surface water. The elemental yield data for Na, Ca, Sr, and Ba obtained in leaching experiments in this study can be used to provide an insight into water-to-rock ratio, as well as the extent to which scaling controls the concentration of these elements in produced waters. To do so we use the published ranges of these elements in produced water from Marcellus Shale gas wells in southwest and north central Pennsylvania (see Table 5 for values used from Rowan et al. (2015) and Gregory et al. (2011)) in the following manner. If water-rock reactions release a fraction (*Y*) of a given element, equation (3) can be written as follows:

$$\frac{W}{R} = \frac{YC_R}{C_{mix} - C_W} \approx \frac{YC_R}{C_{mix}} \tag{4}$$

where we have made the simplification $C_{mix} - C_W \approx C_{mix}$ by noting that $C_{mix} >> C_W$. Here we assume an element-specific value for *Y* based on our leaching experiments (see Table 5). The *W/R* ratio is cast in units L kg^{-1}, and describes the volume of water required to leach one kg of rock to produce the observed concentration in produced water. This model assumes that there is no Ba derived from mixing with formation brine and that the volume of brine is small enough that it would not dilute produced water. We make these simplifications, explicitly, in order to determine if, given only water-rock interactions, it is possible to achieve the Ba concentrations reported in produced water over a reasonable contact time of 7 days. We note that if any formation brine volume were significant relative to injected fluid volume (unlikely, given that only 10–30% of injected volume returns to the well head (Engelder, 2012; King, 2012)), then our calculations would underestimate the contribution of Ba from water-rock interactions.

On an element-by-element basis, the *W/R* ratio describes the relative susceptibility of elemental constituents to removal from the host formation. The *W/R* ratios calculated for Na, Sr, and Ba are similar and of the order of 10^{-2} as shown in Table 5. As the *W/R* ratio for Na, Sr, and Ba are lower than those estimated from Ca by up to one order of magnitude for produced waters on the low end of Ca concentration (Table 5), the key issue is whether the former elements provide a reasonable estimate or are themselves impacted via processes such as scaling. Since produced waters are highly concentrated brines, near-surface precipitation of salts, or scaling reactions, may also impact their elemental concentrations. These salts may include calcite and barite (Crabtree et al., 1999; EPA, 2011, 2014). We note here that our calculations indicate that the Na concentration of the most concentrated brines is still much less than that required for halite precipitation. Thus, Na is likely acting as a conservative ion in the produced water and that the *W/R* ratio estimated using Na could provide a baseline for elements unaffected by removal or fractionation processes.

A low *W/R* ratio is further substantiated by an independent assessment using the geophysical properties of shale. While the effective *W:R* mixing ratio of injected fluids and host rock is difficult to assess in this way, we might estimate a lower limit for the *W/R* ratio (0.01) by assessing the total volume of rock that may physically be accessed by the injected fluid. Here we assume that the total porosity of organic-rich shale (core sample) is ~10.5% of the rock volume and the interconnected porosity that can host water (pre-hydraulic fracturing) is ~3% of the rock volume (Balashov et al., 2015). Since porosity values for hydraulically fractured shale are unknown, porosity for weathered shale taken from outcrop can be used as a first approximation for hydraulically-fractured rock (Balashov et al., 2015). Using a total porosity of 16% and a water-interconnected porosity of 14.5%, the *W/R* ratio derived from weathered shale is 0.06. The *W/R* ratios derived in this manner are similar to those estimated using Na, Sr and Ba as is shown in Table 5.

Stewart et al. (2015) discount the possibility that *W/R* values of ~0.02 could occur during hydraulic fracturing, arguing that the high surface areas of powder samples used in experiments does not accurately represent the surface areas of hydrofractured rock at depth. However, there is no published evaluation of the surface area of the rock involved in water-rock interactions during hydraulic fracturing. Conversely, clay minerals have been shown to be constituents of impoundment sludges that result from the settling of produced water (Zhang et al., 2015a) indicating that abundant fines are produced during hydraulic fracturing. In colloquial terms, anyone that has taken a hammer to shale understands that the particles resulting from fracturing have a wide particle size distribution with many fines produced. The separation of shale fines from both proppant sand and produced liquids is in fact an ongoing endeavor at the industrial scale, as the industry seeks to reduce its waste stream and recycle its products wherever possible. Since the

Table 5
Estimated Water/Rock, *W/R*, mass ratios.

Element	Produced water concentration[a]	Bulk rock concentration[b]	Yield, Y[c]	W/R[d]
Na (low)	18,000	3333 (5000)	0.20	0.04
Na (high)	44,000	3333 (5000)	0.20	0.02
Ca (low)	3000	49,866 (28,000)	0.05	0.83
Ca (high)	31,000	49,866 (28,000)	0.05	0.08
Sr (low)	1400	252 (195)	0.20	0.04
Sr (high)	6800	252 (195)	0.20	0.007
Ba (low)	2300	575 (1127)	0.10	0.03
		5007	0.10	0.02
Ba (high)	6800	575 (1127)	0.10	0.01
		5007	0.10	0.01

[a] Produced water major element ranges are from Gregory et al. (2011) and Rowan et al. (2015); Element concentrations are in μg/mL.
[b] Averages of three Marcellus Shale samples analyzed in this study except in the case for Ba where CC is 5007 μg/g and 575 μg/g is the average of samples without barite (IC and YC); in parentheses are averages of two Marcellus Shale samples analyzed by Balashov et al. (2015). Elemental concentrations are in μg/g.
[c] Element-specific values for *Y* are based on results of leaching experiments (see Table 5).
[d] *W/R* ratios calculated using averages of rock samples analyzed in this study.

surface area of particles scales exponentially with the inverse of particle size it is expected that fines produced during hydraulic fracturing will be the primary contributors of water-rock reaction surface area. Despite the higher surface areas of our powdered samples our experimental *W:R* ratio (50:1) is actually 4 orders of magnitude *higher* than these estimates and thus our experiments are most likely underestimating the amount of Ba released from the rock.

The similarity of *W/R* ratios calculated from Na and Ba also suggests that Ba leaching directly from the rock in anoxic, high salinity solutions is sufficient to achieve the concentrations reported in produced water. However, the *W/R* ratio calculated using Ca is $\geq$ 0.08 or 2 to 42 $\times$ higher than that calculated for Na. This suggests that, with respect to Na, a) there is less Ca present in the MS than estimated here, b) phases containing Ca are less susceptible to mobilization in produced water, or c) the Ca concentration of produced water is much less than that in the fluids initially produced following hydraulic fracturing due to processes that sequester Ca at depth. This suggests that significant amounts of Ca may be precipitating out of solution as calcium carbonate scale before it is sampled. If carbonate is precipitating it should also sequester Sr. However, the *W/R* ratio estimated by Sr is similar to that using Na. This is possible as the Ca/Sr weight ratio in calcite is ~1000–1500. Thus, a hundred fold decrease in Ca via carbonate precipitation will not impact the Sr concentration of produced water. The formation of calcium carbonate and other mineral scale in MS wells is known by industry professionals who list scale inhibitors as one of the most common fracture fluid additives in Marcellus wells (EPA, 2011). However, more studies are required to understand the extent of scale formation at depth.

5. Conclusions

- Between 55 and 75% of the total Ba in organic-rich MS is strongly partitioned into aluminosilicate clays and is only leached from the rock when aluminosilicates are dissolved in hydrofluoric acid.
- Reductive weathering under high ionic strength conditions (i.e., consistent with produced water TDS) releases 5–25% of the total Ba directly from mineral phases within the MS after 7 days.
- Barium is released during reductive weathering under high ionic strength conditions due to: 1) Ba^{2+} in clays exchanging with Na^{+} and Ca^{2+} ions that are present in high concentrations, and 2) increased solubility and dissolution kinetics of barite under high ionic strength conditions.
- Direct leaching from mineral phases within the rock should be treated as a source of Ba in produced water *in addition to* Ba that comes from the possible dilution of basinal brines by injected water.
- Our modeling of water-rock interaction during hydraulic fracturing indicates a water-to-rock ratio of the order of 10^{-2} and that scaling in the producing wells in the Marcellus Basin is dominated by carbonate precipitation.
- In a water-rock interaction scenario, the increasing Ba, Ra and TDS content of produced water that is observed over time may be interpreted as the result of increased contact time and increased water-rock-ratio of later fluids.

Acknowledgments

The authors would like to thank Jim Leone and Charles Ver Straeten at the New York State Museum in Albany, NY and Katie Schmid the Pennsylvania Department of Conservation and Natural Resources for providing samples. Special thanks to Robert Brandom and Ted Juzwak (Bruker) for assistance with μ-XRF analysis.

Appendix A. Supplementary data

Supplementary data related to this article can be found at http://dx.doi.org/10.1016/j.apgeochem.2015.11.001.

References

Akob, D.M., Cozzarelli, I.M., Dunlap, D.S., Rowan, E.L., Lorah, M.M., 2015. Organic and inorganic composition and microbiology of produced waters from Pennsylvania shale gas wells. Appl. Geochem 115–125.
Atun, G., Bascetin, E., 2003. Adsorption of barium on kaolinite, illite and montmorillonite at various ionic strengths. Radiochim. Acta 223–228.
Balashov, V.N., Engelder, T., Gu, X., Fantle, M.S., Brantley, S.L., 2015. A model describing flowback chemistry changes with time after Marcellus Shale hydraulic fracturing. AAPG Bull. 143–154.
Baldi, F., Pepi, M., Burrini, D., Kniewald, G., Scali, D., Lanciotti, E., 1996. Dissolution of barium from barite in sewage sludges and cultures of desulfovibrio desulfuricans. Appl. Environ. Microbiol. 2398–2404.
Bazant, Z.P., Salviato, M., Chau, V.T., Viswanathan, H., Zubelewicz, A., 2014. Why fracking works. J. Appl. Mech. Trans. ASME 81.
Blauch, M.E., Myers, R.R., Moore, T.R., Lipinski, B.A., Houston, N.A., 2009. Marcellus Shale Post-frac Flowback Waters: Where Is All the Salt Coming from and What are the Implications? Society of Petroleum Engineers, p. 20. SPE 125740.
Blount, C.W., 1977. Barite solubilities and thermodynamic quantities up to 300-degrees-C and 1400-bars. Am. Min. 942–957.
Capo, R.C., Stewart, B.W., Rowan, E.L., Kohl, C.A.K., Wall, A.J., Chapman, E.C., Hammack, R.W., Schroeder, K.T., 2014. The strontium isotopic evolution of Marcellus formation produced waters, southwestern Pennsylvania. Int. J. Coal Geol. 57–63.
Chapman, E.C., Capo, R.C., Stewart, B.W., Kirby, C.S., Hammack, R.W., Schroeder, K.T., Edenborn, H.M., 2012. Geochemical and strontium isotope characterization of produced waters from Marcellus Shale natural gas extraction. Environ. Sci. Technol. 3545–3553.
Chen, J.H., Edwards, R.L., Wasserburg, G.J., 1986. U-238,U-234 and TH-232 in

seawater. Earth Planet S. C. Lett. 241–251.
Cluff, M.A., Hartsock, A., MacRae, J.D., Carter, K., Mouser, P.J., 2014. Temporal changes in microbial ecology and geochemistry in produced water from hydraulically fractured Marcellus Shale gas wells. Environ. Sci. Technol. 6508–6517.
Coffey, M., Dehairs, F., Collette, O., Luther, G., Church, T., Jickells, T., 1997. The behaviour of dissolved barium in estuaries. Estuar. Coast. Shelf Sci. 113–121.
Cohen, A.S., Onions, R.K., 1991. Precise determination of femtogram quantities of radium by thermal ionization mass-spectrometry. Anal. Chem. 2705–2708.
Crabtree, M., Eslinger, D., Fletcher, P., Miller, M., Johnson, A., King, G., 1999. Fighting scale – removal and prevention. Oilfield Rev. – Schlumb. 30–45.
Cronan, C.S., Schofield, C.L., 1979. Aluminum leaching response to acid precipitation – effects on high-elevation watersheds in the Northeast. Science 304–306.
Dresel, P.E., Rose, A.W., 2010. Chemistry and origin of oil and gas well brines in Western Pennsylvania. Pa. Geol. Surv. Open-File Rep. 48.
Dymond, J., Suess, E., Lyle, M., 1992. Barium in deep-sea sediment: a geochemical proxy for paleoproductivity. Paleoceanography 163–181.
Eagle, M., Paytan, A., Arrigo, K.R., van Dijken, G., Murray, R.W., 2003. A comparison between excess barium and barite as indicators of carbon export. Paleoceanography 18.
Engelder, T., 2012. Capillary tension and imbibition sequester frack fluid in Marcellus gas shale. Proc. Natl. Acad. Sci. U. S. A. 109 (12), E3625.
Engelder, T., Cathles, L.M., Bryndzia, L.T., 2014. The fate of residual treatment water in gas shale. J. Unconv. Oil Gas Resour. 33–48.
Engle, M.A., Rowan, E.L., 2014. Geochemical evolution of produced waters from hydraulic fracturing of the Marcellus Shale, northern Appalachian Basin: a multivariate compositional data analysis approach. Int. J. Coal Geol. 45–56.
EPA, 2011. In: Proceedings of the Technical Workshops for the Hydraulic Fracturing Study: Chemical and Analytical Methods, Washington DC.
EPA, 2014. In: Agency, U.S.E.P. (Ed.), EPA's Study of Hydraulic Fracturing for Oil and Gas and its Potential Impact on Drinking Water Resources.
Evans, M.A., 1995. Fluid inclusions in veins from the middle Devonian Shales – a record of deformation conditions and fluid evolution in the Appalachian Plateau. Geol. Soc. Am. Bull. 327–339.
Farquhar, J., Bao, H.M., Thiemens, M., 2000. Atmospheric influence of Earth's earliest sulfur cycle. Science 756–758.
Gingele, F., Dahmke, A., 1994. Discrete barite particles and barium as tracers of paleoproductivity in south-atlantic sediments. Paleoceanography 151–168.
Gregory, K.B., Vidic, R.D., Dzombak, D.A., 2011. Water management challenges associated with the production of shale gas by hydraulic fracturing. Elements 181–186.
Haluszczak, L.O., Rose, A.W., Kump, L.R., 2013. Geochemical evaluation of flowback brine from Marcellus gas wells in Pennsylvania, USA. Appl. Geochem. 55–61.
Hamlat, M.S., Kadi, H., Fellag, H., 2003. Precipitate containing norm in the oil industry: modelling and laboratory experiments. Appl. Radiat. Isotopes 95–99.
Hosterman, J.W., Whitlow, S., 1983. Clay Mineralogy of Devonian Shales – a Record of Deformation Conditions and Fluid Evolution in the Appalachian Plateau. United States Geological Survey, Washington, DC, p. 36.
King, G.E., 2012. Hydraulic fracturing 101: what every representative, environmentalist, regulator, reporter, investor, university researcher, neighbor, and engineer should know about estimating frac risk and improving frac performance in unconventional gas and oil wells. J. Pet. Technol. 34–42.
Klump, J., Hebbeln, D., Wefer, G., 2000. The impact of sediment provenance on barium-based productivity estimates. Mar. Geol. 259–271.
Kohl, C.A.K., Capo, R.C., Stewart, B.W., Wall, A.J., Schroeder, K.T., Hammack, R.W., Guthrie, G.D., 2014. Strontium isotopes test long-term zonal isolation of injected and Marcellus formation water after hydraulic fracturing. Environ. Sci. Technol. 9867–9873.
Kowacz, M., Putnis, A., 2008. The effect of specific background electrolytes on water structure and solute hydration: consequences for crystal dissolution and growth. Geochim. Cosmochim. Ac 4476–4487.
Landis, J., Sharma, M., Renock, D., 2015. Origin of Radium Orphaned during Hydraulic Fracturing. Geological Society of America, Baltimore, MD.
Lash, G.G., Blood, D.R., 2014. Organic matter accumulation, redox, and diagenetic history of the Marcellus formation, southwestern Pennsylvania, Appalachian basin. Mar. Pet. Geol. 244–263.
Monnin, C., 1995. Thermodynamic Model for the Solubility of Barite and Celestite in Natural Waters from 0 to 200 Degrees C and to 1 Kbar.
Monnin, C., 1999. A thermodynamic model for the solubility of barite and celestite in electrolyte solutions and seawater to 200 degrees C and to 1 kbar. Chem. Geol. 187–209.
Monnin, C., Galinier, C., 1988. The solubility of celestite and barite in electrolyte-solutions and natural-waters at 25-degrees-C - a thermodynamic study. Chem. Geol. 283–296.
Niu, D., Renock, D., Whitehouse, M., Symcox, C.W., Hamren, K., Leone, J., Landis, J., Sharma, M., 2015. A relict sulfate-methane transition zone in the mid-Devonian Marcellus Shale (in review). Geochim. Cosmochim. Acta.
Osborn, S.G., McIntosh, J.C., 2010. Chemical and isotopic tracers of the contribution of microbial gas in devonian organic-rich shales and reservoir sandstones, northern Appalachian Basin. Appl. Geochem. 456–471.
Osborn, S.G., McIntosh, J.C., Hanor, J.S., Biddulph, D., 2012. Iodine-129, Sr-87/Sr-86, and trace elemental geochemistry of northern Appalachian Basin brines: evidence for basinal-scale fluid migration and clay mineral diagenesis. Am. J. Sci. 263–287.
Osborn, S.G., Vengosh, A., Warner, N.R., Jackson, R.B., 2011. Methane contamination of drinking water accompanying gas-well drilling and hydraulic fracturing. Proc. Natl. Acad. Sci. U. S. A. 8172–8176.
Phan, T.T., Capo, R.C., Stewart, B.W., Graney, J.R., Johnson, J.D., Sharma, S., Tora, J., 2015. Trace metal distribution and mobility in drill cuttings and produced waters from Marcellus shale gas extraction: uranium, arsenic, barium. Appl. Geochem. 89–103.
Pirrung, M., Illner, P., Matthiessen, J., 2008. Biogenic barium in surface sediments of the European Nordic Seas. Mar. Geol. 89–103.
Risthaus, P., Bosbach, D., Becker, U., Putnis, A., 2001. Barite scale formation and dissolution at high ionic strength studied with atomic force microscopy. Coll. Surfaces a-Physicochem. Eng. Aspects 201–214.
Rowan, E.L., Engle, M.A., Kirby, C.S., Kraemer, T.F., 2011. In: Radium Content of Oil- and Gas-field Produced Waters in the Northern Appalachian Basin (USA): Summary and Discussion of Data. Geological Survey, U.S., p. 31. Scientific Investigations Report 2011-5135.
Rowan, E.L., Engle, M.A., Kraemer, T.F., Schroeder, K.T., Hammack, R.W., Doughten, M.W., 2015. Geochemical and isotopic evolution of water produced from middle Devonian Marcellus shale gas wells, Appalachian basin, Pennsylvania. Aapg Bull. 181–206.
Srodon, J., Drits, V.A., McCarty, D.K., Hsieh, J.C.C., Eberl, D.D., 2001. Quantitative X-ray diffraction analysis of clay-bearing rocks from random preparations. Clay Clay Min. 514–528.
Stewart, B.W., Chapman, E.C., Capo, R.C., Johnson, J.D., Graney, J.R., Kirby, C.S., Schroeder, K.T., 2015. Origin of brines, salts and carbonate from shales of the Marcellus formation: evidence from geochemical and Sr isotope study of sequentially extracted fluids. Appl. Geochem. 78–88.
Stueber, A.M., Walter, L.M., 1991. Origin and chemical evolution of formation waters from Silurian-Devonian strata in the Illinois basin, USA. Geochim. Cosmochim. Ac 309–325.
Vidic, R.D., Brantley, S.L., Vandenbossche, J.M., Yoxtheimer, D., Abad, J.D., 2013. Impact of shale gas development on regional water quality. Science 340 (6134).
Wang, G., Carr, T.R., December 2013. Organic-rich Marcellus shale lithofacies modeling and distribution pattern analysis in the Appalachian Basin. AAPG Bull. 97 (12), 2173–2205.
Warner, N.R., Christie, C.A., Jackson, R.B., Vengosh, A., 2013. Impacts of shale gas wastewater disposal on water quality in Western Pennsylvania. Environ. Sci. Technol. 11849–11857.
Warner, N.R., Jackson, R.B., Darrah, T.H., Osborn, S.G., Down, A., Zhao, K.G., White, A., Vengosh, A., 2012. Geochemical evidence for possible natural migration of Marcellus formation brine to shallow aquifers in Pennsylvania. Proc. Natl. Acad. Sci. U. S. A. 11961–11966.
Weary, D.J., Ryder, R.T., Nyahay, R.E., 2001. Thermal Maturity Patterns in New York State Using CAI and %Ro, Northeastern Geology and Environmental Sciences. Northeastern Science Foundation, Inc., pp. 356–376
Wedepohl, W.K., 1971. Environmental Influences on the Chemical Composition of Shales and Clays. Pergamon, Oxford.
Werne, J.P., Sageman, B.B., Lyons, T.W., Hollander, D.J., 2002. An integrated assessment of a “type euxinic” deposit: evidence for multiple controls on black shale deposition in the middle Devonian oatka creek formation. Am. J. Sci. 110–143.
Wilhelm, M., Cobb, L.B., 1981. Coring and Logging of EGSP Pennsylvania Well No.4 Indiana County, Pennsylvania, Eastern Gas Shales Project. Department of Energy, Houston, Texas.
Zhang, P.C., Brady, P.V., Arthur, S.E., Zhou, W.Q., Sawyer, D., Hesterberg, D.A., 2001. Adsorption of barium(II) on montmorillonite: an EXAFS study. Coll. Surfaces a-Physicochem. Eng. Aspects 239–249.
Zhang, T., Hammack, R.W., Vidic, R.D., 2015a. Fate of radium in Marcellus shale flowback water impoundments and assessment of associated health risks. Environ. Sci. Technol. Am. Chem. Soc. 9347–9354.
Zhang, T., Hammack, R.W., Vidic, R.D., 2015b. Fate of radium in Marcellus shale flowback water impoundments and assessment of associated health risks. Environ. Sci. Technol. 49 (15), 9347–9354.
Zhu, C., 2004. Coprecipitation in the Barite isostructural family: 1. Binary mixing properties. Geochim. Cosmochim. Ac 3327–3337.